Letters

Modeling of a Three-Phase ZVS Mixed Conduction Mode DC–AC Inverter Into Equivalent Single-Phase DC–AC Inverters

Sungjae Ohn, Nidhi Haryani, *Member, IEEE*, Rolando Burgos, *Senior Member, IEEE*, and Dushan Boroyevich, *Life Fellow, IEEE*

***Abstract*—To achieve zero-voltage switching (ZVS), triangular conduction mode (TCM) delays the turn-OFF time of SiC MOSFETs to generate a reverse current that discharges the junction capacitance–voltage before a MOSFET turns ON. In the literature, TCM has been combined with discontinuous conduction mode (DCM) and discontinuous pulsewidth modulation to achieve ZVS in three-phase inverters. However, the coupling between the three phases, and transitions between the different modes cause complexity in the modeling and current control. This article presents a simple modeling approach where the modeling and analysis for an equivalent single-phase TCM and DCM inverter can be directly extended to this mixed conduction mode. Thanks to the simplicity, not only the impact of the three-phase coupling can be compensated, but also small signal gains for current control can easily be derived. The proposed modeling approach has been verified by SIMPLIS simulation and experimental tests with a three-phase PV inverter.**

***Index Terms*—Small signal modeling, soft switching, triangular conduction mode (TCM).**

I. Introduction

WIDE-BANDGAP (WBG) devices, such as silicon carbide (SiC), have expanded their market share for grid-connected applications, as shown in Fig. 1. The switching loss of SiC devices is reported to be concentrated at a turn-ON instant. Therefore, if turn-ON loss can be eliminated through zero-voltage switching (ZVS), the switching frequency can be elevated and the power density of the photovoltaic inverter can be significantly improved. Triangular conduction mode (TCM) is one of the ZVS methods for single-phase dc–ac inverter [1], [2], [3], [4], [5]. By extending the turn-OFF time, ZVS can be achieved without any auxiliary circuitry.

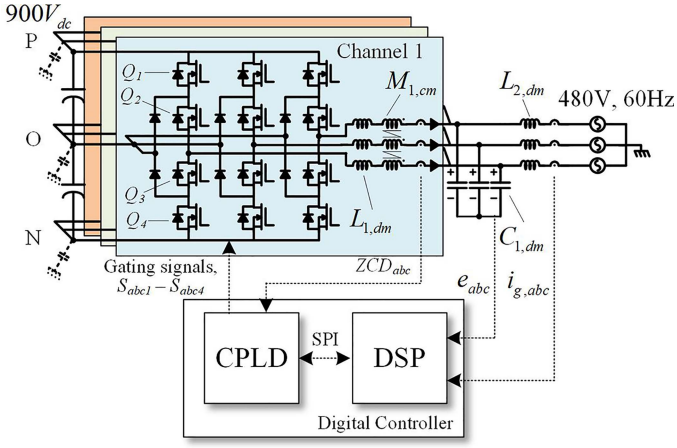

Fig. 1. Circuit for a three-phase three-level inverter for photovoltaic applications.

However, in three-phase applications, all phases are coupled through the neutral point of the load. This coupling complicates the analysis of the current slope for the TCM operation. In [6], [7], [8], and [9], additional capacitors are inserted to run three phases independently. However, the filter inductors are exposed to a wide switching frequency variation, and the modulation index (MI) range is limited.

To increase the MI range and narrow down the variation of the switching frequency, a modulation with mixed conduction mode is proposed [10], [11], [12], namely, TCM, discontinuous conduction mode (DCM), and discontinuous pulsewidth modulation (DPWM). While one phase is clamped to positive or negative dc-rail, the other two operate in TCM and DCM. The conduction mode for each phase alternates according to the angle of current reference and the variation of switching frequency is narrow. However, the detailed modeling of such a modulation scheme has not been investigated. Especially, how the three-phase coupling will impact the current slope, thus the dynamics of TCM, and DCM operation is not clear.

In this article, a single-phase equivalent model for this mixed conduction mode modulation has been presented. The modeling approach decomposes the three-phase inverter into two independent single-phase inverters. Such an approach not only significantly simplifies the analysis of the modulation but also

Received 3 May 2024; revised 7 June 2024 and 4 July 2024; accepted 26 July 2024. Date of publication 15 August 2024; date of current version 7 October 2024. This work was supported in part by the Office of Energy Efficiency and Renewable Energy (EERE), U.S. Department of Energy, under Award DEEE0006521 with North Carolina State University, Power America Institute. *(Corresponding author: Sungjae Ohn.)*

Sungjae Ohn is with the Bradley Department of Electrical and Computer Engineering, Virginia Tech, Arlington, VA 22203 USA, and also with the Tesla, Inc., Austin, TX 78725 USA (e-mail: ohn@vt.edu).

Nidhi Haryani is with the Delta Electronics, Durham, NC 27709 USA (e-mail: nidhi05@vt.edu).

Rolando Burgos and Dushan Boroyevich are with the Bradley Department of Electrical and Computer Engineering, Virginia Tech, Blacksburg, VA 24060 USA (e-mail: burgos@vt.edu; dushan@vt.edu).

Color versions of one or more figures in this article are available at https://doi.org/10.1109/TPEL.2024.3441655.

Digital Object Identifier 10.1109/TPEL.2024.3441655

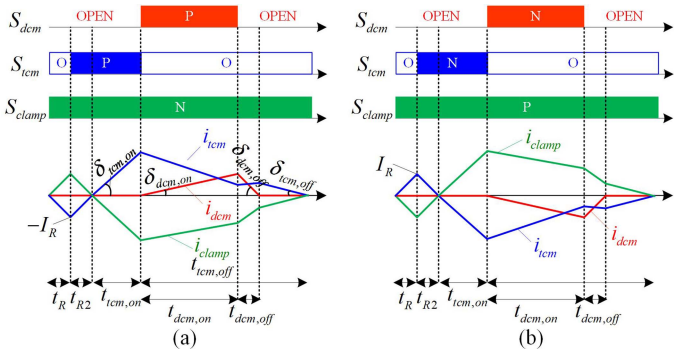

Fig. 2. Switching sequences to achieve ZVS for the three-level three-phase inverter. (a) DPWM phase to the negative dc-rail case. (b) DPWM phase to the positive dc-rail case.

TABLE I
DEFINITION OF SWITCHING STATES

Switching state	Q1	Q2	Q3	Q4
P	ON	ON	OFF	OFF
O	OFF	ON	ON	OFF
N	OFF	OFF	ON	ON
OPEN	OFF	OFF	OFF	OFF

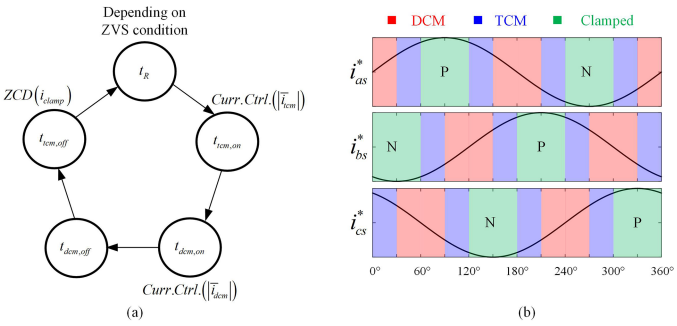

Fig. 3. (a) State diagram of the switching sequence. (b) Transition of three different conduction modes for ZVS of three phases.

enables the control scheme for the single-phase inverters to be extended to the mixed conduction mode modulation, such as closed-loop interleaving. The proposed modeling is verified with SIMPLIS simulation and experimental results.

II. Switching Sequence for ZVS Operation

In this section, the switching sequence under study as Fig. 2 is briefly explained. The switching state of the three-level phase leg is summarized in Table I. The conduction mode for each phase is determined by the sector of the current reference, as shown in Fig. 3(b). Due to the symmetry in the three-phase system, the switching sequence can be classified into only two cases, as shown in Fig. 2. The difference between the two cases is in the DPWM. "P" and "N" for the DPWM indicate the direction of the clamping, similar to DPWM60.

By the switching of the other two phases, the DPWM phase current (i_{clamp}) is determined through the three-phase coupling. In both cases, the zero-crossing detection (ZCD) of i_{clamp} is used as an indicator for the beginning of the next switching cycle [10], [11], [12]. The state diagram is shown in Fig. 3(a).

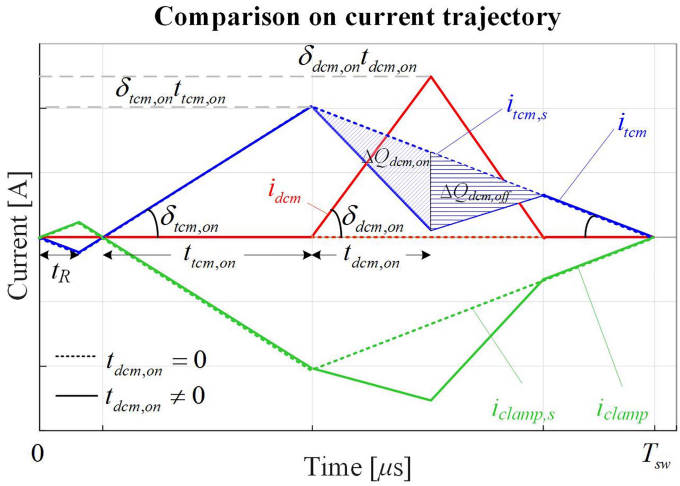

Fig. 4. Comparison of current trajectory depending on DCM phase switching.

For the DCM phase, the MOSFETs remain open except for ON-time $(t_{\text{dcm,on}})$. The $t_{\text{dcm,on}}$ is placed at the beginning of the OFF-time of the TCM phase $(t_{\text{tcm,off}})$ in Fig. 2, and determines the average current $(\bar{i}_{\text{dcm}})$.

For TCM phase, the TCM phase current (i_{tcm}) is built up, during TCM phase ON-time $(t_{\text{tcm,on}})$, and goes back to zero during $t_{\text{tcm,off}}$. The value of $t_{\text{tcm,on}}$ determines the average value of i_{tcm} $(\bar{i}_{\text{tcm}})$. However, due to the DCM phase, the slope of i_{tcm} changes. TCM OFF-time with "O" state is extended by t_R, and generates a reverse current (I_R). The total switching period (t_{sw}) can be written as

$$t_{\text{sw}} = t_R + t_{R2} + t_{\text{tcm,on}} + t_{\text{tcm,off}}. \tag{1}$$

III. Impact of Three-Phase Coupling

Since the dynamics of the TCM operation largely rely on the current slope and zero-current detection (ZCD) instant, the analysis, and control for the single-phase TCM inverter cannot be directly extended to the mixed mode modulation. This section reveals an intuitive understanding on the impact of the three-phase coupling on t_{sw}, and the average currents.

Except for $t_{\text{dcm,on}}$ and $t_{\text{dcm,off}}$, no MOSFETs or diodes on the DCM phase are ON, and the TCM and DPWM phase operate like a single-phase TCM inverter. When the DCM phase doesn't switch, di/dt of i_{tcm} is defined as $\delta_{\text{tcm,on}}$ and $\delta_{\text{tcm,off}}$, as shown in Fig. 4, where e_{tcm}, e_{dcm}, and e_{clamp} are the grid voltages across the filter capacitor $(C_{1,dm})$ of the corresponding conduction mode, and $L_{1,dm}$ is the filter inductance. The polarity of the clamping direction is represented by Pol as

$$\text{Pol} = \begin{cases} 1, & \text{if clamping is toward P} \\ -1, & \text{if clamping is toward N.} \end{cases} \tag{2}$$

Similarly, di/dt of i_{dcm} is defined as $\delta_{\text{dcm,on}}$ and $\delta_{\text{dcm,off}}$. The equations for these current slopes are summarized in Table II. The impact from the three-phase coupling occurs during $t_{\text{dcm,on}}$ and $t_{\text{dcm,off}}$. Considering half of the DCM current flows into the other two phases and based on Table II, the di/dt of all three phases can be written as Table III.

TABLE II
EQUATIONS FOR CURRENT SLOPES

Current slope	Equation
$\delta_{\text{tcm,on}}$	$\frac{Pol*V_{\text{dc}}-(e_{\text{tcm}}-e_{\text{clamp}})}{2L_{1,dm}}$
$\delta_{\text{tcm,off}}$	$\frac{Pol*V_{\text{dc}}/2-(e_{\text{tcm}}-e_{\text{clamp}})}{2L_{1,dm}}$
$\delta_{\text{dcm,on}}$	$\frac{Pol*V_{\text{dc}}/2-e_{\text{dcm}}}{L_{1,dm}}$
$\delta_{\text{dcm,off}}$	$\frac{-Pol*V_{\text{dc}}/6-e_{\text{dcm}}}{L_{1,dm}}$

TABLE III
SUMMARY OF CURRENT SLOPES FOR EACH PERIOD

Time period	TCM phase	DCM phase	DPWM phase
$t_{\text{tcm,on}}$	$\delta_{\text{tcm,on}}$	N/A	$-\delta_{\text{tcm,on}}$
$t_{\text{dcm,on}}$	$\delta_{\text{tcm,off}}-\frac{\delta_{\text{dcm,on}}}{2}$	$\delta_{\text{dcm,on}}$	$-\delta_{\text{tcm,off}}-\frac{\delta_{\text{dcm,on}}}{2}$
$t_{\text{dcm,off}}$	$\delta_{\text{tcm,off}}-\frac{\delta_{\text{dcm,off}}}{2}$	$\delta_{\text{dcm,off}}$	$-\delta_{\text{tcm,off}}-\frac{\delta_{\text{dcm,off}}}{2}$
Rest of t_{sw}	$\delta_{\text{tcm,off}}$	N/A	$-\delta_{\text{tcm,off}}$

A. Switching Period, t_{sw}

The DCM phase returns to zero as (3) after $t_{\text{dcm,off}}$. The value of the TCM current after the DCM phase turns OFF ($i_{\text{tcm}}|_{t=t_{\text{dcm,off}}}$) can be simplified as (4)

$$\delta_{\text{dcm,on}}t_{\text{dcm,on}}+\delta_{\text{dcm,off}}t_{\text{dcm,off}}=0 \tag{3}$$

$$i_{\text{tcm}}|_{t=t_{\text{dcm,off}}}=\delta_{\text{tcm,on}}t_{\text{tcm,on}}+\delta_{\text{tcm,off}}(t_{\text{dcm,on}}+t_{\text{dcm,off}}). \tag{4}$$

An important observation can be made from (4). First, since i_{dcm} goes back to zero, $i_{\text{tcm}}|_{t=t_{\text{dcm,off}}}$ does not change whether the DCM phase is switched or not. This is visualized with the simulation waveform in Fig. 4. The currents of the TCM and DPWM phase without the DCM phase operation are labeled as $i_{\text{tcm},s}$, and $i_{\text{clamp},s}$.

B. Average Currents

From its triangular shape, the average value of i_{dcm} can be derived as (5). The loss of charge on i_{tcm} compared to $i_{\text{tcm},s}$ during $t_{\text{dcm,on}}$ ($\Delta Q_{\text{dcm,on}}$) and $t_{\text{dcm,off}}$ ($\Delta Q_{\text{dcm,off}}$) can be calculated. The value of $\Delta Q_{\text{dcm,on}}+\Delta Q_{\text{dcm,off}}$ equals the half of $\bar{i}_{\text{dcm}}t_{\text{sw}}$ as (6). This confirms that when the DCM phase operates, the impact on the average current will be that the $\bar{i}_{\text{dcm}}$ is split to the TCM and DPWM phase by a half.

$$\bar{i}_{\text{dcm}}=\frac{t_{\text{dcm,on}}^2}{2t_{\text{sw}}}\delta_{\text{dcm,on}}\left(1-\frac{\delta_{\text{dcm,on}}}{\delta_{\text{dcm,off}}}\right) \tag{5}$$

$$\Delta Q_{\text{dcm,on}}+\Delta Q_{\text{dcm,off}}=-\frac{\bar{i}_{\text{dcm}}}{2}t_{\text{sw}}. \tag{6}$$

It is important to note that the derivation process does not include the impact of resonance between C_{oss} and $L_{1,dm}$ during the dead time. When the energy stored in $L_{1,dm}$ by I_R is not sufficient to discharge C_{oss}, non-ZVS may occur on the TCM phase. More importantly, if these resonance periods take a significant portion of t_{sw}, the impact on the average current may become notable. For the given condition in this letter, dead time is 200 ns and the average t_{sw} within one line cycle is around 7μs. Therefore, the impact of the resonance period on $\bar{i}_{\text{tcm}}$ and $\bar{i}_{\text{dcm}}$ was not significant.

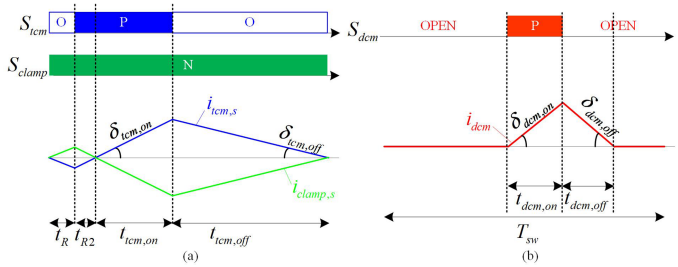

Fig. 5. Decomposition of three-phase TCM inverter. (a) Equivalent single-phase TCM inverter. (b) Equivalent single-phase DCM inverter.

TABLE IV
ANALYTIC SOLUTIONS FOR THE AVERAGE CURRENTS

Variables	Equation
t_{sw}	$t_R(1-\frac{\delta_{\text{tcm,off}}}{\delta_{\text{tcm,on}}})+t_{\text{tcm,on}}\ (1-\frac{\delta_{\text{tcm,on}}}{\delta_{\text{tcm,off}}})$
Q_R	$\frac{t_R^2}{2}\delta_{\text{tcm,off}}\ (1-\frac{\delta_{\text{tcm,off}}}{\delta_{\text{tcm,on}}})$
$\bar{i}_{\text{tcm},s}$	$\frac{t_{\text{tcm,on}}^2}{2t_{\text{sw}}}\delta_{\text{tcm,on}}\ (1-\frac{\delta_{\text{tcm,on}}}{\delta_{\text{tcm,off}}})+\frac{Q_R}{t_{\text{sw}}}$
$\bar{i}_{\text{dcm}}$	$\frac{t_{\text{dcm,on}}^2}{2t_{\text{sw}}}\delta_{\text{dcm,on}}\ (1-\frac{\delta_{\text{dcm,on}}}{\delta_{\text{dcm,off}}})$
$\bar{i}_{\text{tcm}}$	$\bar{i}_{\text{tcm,s}}-\bar{i}_{\text{dcm}}/2$
$\bar{i}_{\text{clamp}}$	$-\bar{i}_{\text{tcm,s}}-\bar{i}_{\text{dcm}}/2$

IV. PROPOSED SINGLE-PHASE EQUIVALENT CIRCUIT MODELING

The impact of three-phase coupling can be understood based on Sections III-A and III-B. The DCM phase does not change t_{sw}, and t_{sw} can be calculated from the single-phase TCM inverter with the filter inductance of $2L_{1,dm}$. With given t_{sw}, the DCM phase turns ONfor $t_{\text{dcm,on}}$ to build a triangular current, and, in terms of the average current, $\bar{i}_{\text{dcm}}$ is split to the TCM and clamped phase by a half.

According to these observations, the waveforms of an equivalent single-phase TCM inverter with the same $\delta_{\text{tcm,on}}$ and $\delta_{\text{tcm,off}}$ are drawn in Fig. 5(a). The average current of $i_{\text{tcm},s}$ ($\bar{i}_{\text{tcm},s}$) can be calculated as Table IV, where Q_R refers to the loss on the charge by the reverse current. The switching period is written by a function of t_R, $t_{\text{tcm,on}}$, $\delta_{\text{tcm,on}}$, and $\delta_{\text{tcm,off}}$, and independent of the DCM phase. All 12 sectors in Fig. 3(b) can be considered by reflecting the change into $\delta_{\text{tcm,on}}$, $\delta_{\text{dcm,on}}$, $\delta_{\text{tcm,off}}$, and $\delta_{\text{dcm,off}}$

With given t_{sw}, the waveforms of an equivalent singe-phase DCM inverter with the same $\delta_{\text{dcm,on}}$ and $\delta_{\text{dcm,off}}$ are drawn in Fig. 5(b). The average current is the same as (5).

The average currents ($\bar{i}_{\text{dcm}}$, $\bar{i}_{\text{tcm}}$, and $\bar{i}_{\text{clamp}}$) are a superposition of the equivalent TCM and DCM inverters, as shown in Table IV. Thanks to the simplicity of the analytic expressions, analytic solutions for the small-signal gain ($\Delta\bar{i}_{\text{tcm}}/\Delta t_{\text{tcm,on}}, \Delta\bar{i}_{\text{dcm}}/\Delta t_{\text{dcm,on}}$) can be derived in the following three steps: large signal model, perturbation, and linearization. Large signal operating points and perturbations can be written as follows:

$$t_{\text{sw}}=T_{\text{sw}}+\Delta t_{\text{sw}}$$

$$t_{\text{tcm,on}}=T_{\text{tcm,on}}+\Delta t_{\text{tcm,on}}$$

TABLE V
ANALYTIC SOLUTIONS FOR SMALL SIGNAL GAIN

Variables	Equation
$\Delta t_{\rm sw}/\Delta t_{\rm tcm,on}$	$1-\frac{\delta_{\rm tcm,on}}{\delta_{\rm tcm,off}}$
$\Delta\bar{i}_{\rm dcm}/\Delta t_{\rm dcm,on}$	$\frac{T_{\rm dcm,on}}{T_{\rm sw}}\delta_{\rm dcm,on}(1-\frac{\delta_{\rm dcm,on}}{\delta_{\rm dcm,off}})$
$\Delta\bar{i}_{\rm dcm}/\Delta t_{\rm tcm,on}$	$-\frac{\bar{I}_{\rm dcm}}{T_{\rm sw}}(1-\frac{\delta_{\rm tcm,on}}{\delta_{\rm tcm,off}})$
$\Delta\bar{i}_{\rm tcm}/\Delta t_{\rm tcm,on}$	$\frac{T_{\rm tcm,on}}{T_{\rm sw}}\delta_{\rm tcm,on}(1-\frac{\delta_{\rm tcm,on}}{\delta_{\rm tcm,off}})-\frac{T_{\rm tcm,on}^2}{2T_{\rm sw}^2}\delta_{\rm tcm,on}(1-\frac{\delta_{\rm tcm,on}}{\delta_{\rm tcm,off}})^2$ $-\frac{\bar{I}_{\rm dcm}}{T_{\rm sw}}(1-\frac{\delta_{\rm tcm,on}}{\delta_{\rm tcm,off}})-\frac{Q_R}{T_{\rm sw}^2}(1-\frac{\delta_{\rm tcm,on}}{\delta_{\rm tcm,off}})$
$\Delta\bar{i}_{\rm tcm}/\Delta t_{\rm dcm,on}$	$-\frac{1}{2}\frac{\Delta\bar{i}_{\rm dcm}}{\Delta t_{\rm dcm,on}}$

TABLE VI
ANALYTIC SOLUTIONS FOR $t^*_{\rm tcm,on}, t^*_{\rm dcm,on}$ GIVEN $\bar{i}^*_{\rm tcm}, \bar{i}^*_{\rm dcm}$

Variables	Equation
$t^*_{\rm tcm,on}$	$\sqrt{\frac{2T_{\rm sw}}{\delta_{\rm tcm,on}(1-\frac{\delta_{\rm tcm,on}}{\delta_{\rm tcm,off}})}(\bar{i}^*_{\rm tcm}+\frac{\bar{i}^*_{\rm dcm}}{2}-\frac{Q_R}{T_{\rm sw}})}$
$t^*_{\rm dcm,on}$	$\sqrt{\frac{2T_{\rm sw}}{\delta_{\rm dcm,on}(1-\frac{\delta_{\rm dcm,on}}{\delta_{\rm dcm,off}})}\bar{i}^*_{\rm dcm}}$

TABLE VII
PARAMETERS FOR THE THREE-PHASE PV INVERTER IN TCM

Parameter	Value	Parameter	Value
$V_{\rm dc}$	900 V	V_{ac}	480 V
$L_{1,dm}$	7 μH	C_{oss}	40 nF
$f_{\rm sw}$	140 kHz	t_R	0 μs

$$t_{\rm dcm,on} = T_{\rm dcm,on} + \Delta t_{\rm dcm,on}$$
$$\bar{i}_{\rm tcm} = \bar{I}_{\rm tcm} + \Delta\bar{i}_{\rm tcm}$$
$$\bar{i}_{\rm dcm} = \bar{I}_{\rm dcm} + \Delta\bar{i}_{\rm dcm}. \quad (7)$$

Small signal gains can be calculated by replacing (7) into Table IV. Second-order terms (multiple of two perturbation terms) are removed to linearize equations. The summary is provided in Table V.

In practical implementation, $T_{\rm sw}$ varies slowly over the fundamental cycle and the processor can easily read back $T_{\rm sw}$ from a complex programmable logic device (CPLD) in Fig. 1. When the reference values for $\bar{i}_{\rm dcm}$ and $\bar{i}_{\rm tcm}$ (labeled as $\bar{i}^*_{\rm dcm}$ and $\bar{i}^*_{\rm tcm}$) are given, the feedforward value for $t_{\rm tcm,on}$ and $t_{\rm dcm,on}$ ($t^*_{\rm tcm,on}, t^*_{\rm dcm,on}$) can be calculated, as given Table VI. More details on the current controller implementation can be found under [13].

V. SIMULATION RESULT

SIMPLIS simulation has been designed to extract the small signal gains. The schematic for SIMPLIS simulation is shown in Fig. 6. The parameters for the simulation are summarized in Table VII. When the three-phase TCM inverter operates between 0° and 30° with unity power factor, four small signal gains at 0°, 5°, 10°, 15°, 20°, 25° and 30° are simulated. The results are shown in Fig. 7.

To validate the model, the small-signal gains are calculated based on analytic solutions in Table V, and their magnitude is compared with the simulation result in Fig. 8. The model does not predict the sub-harmonic oscillation near $f_{\rm sw}$; only low-frequency gain <2 kHz for digital control has been compared, and shown in Fig. 8. The proposed model can accurately predict

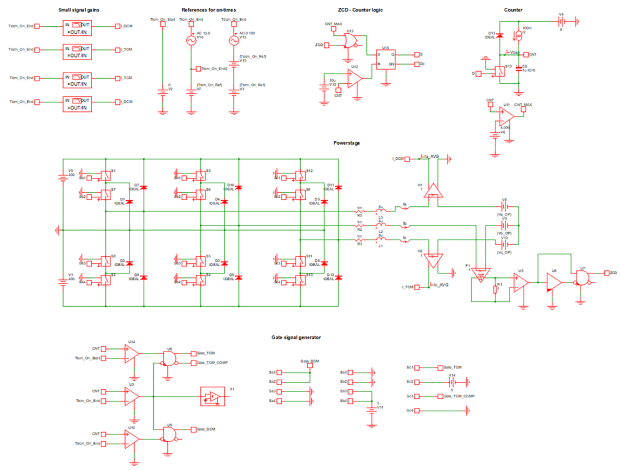

Fig. 6. Schematic for SIMPLIS simulation.

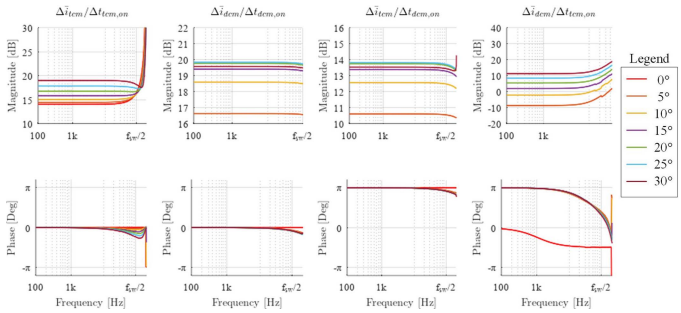

Fig. 7. Bode plots of small-signal gains from SIMPLIS: $\Delta\bar{i}_{\rm tcm}/\Delta t_{\rm tcm,on}$, $\Delta\bar{i}_{\rm dcm}/\Delta t_{\rm dcm,on}$, $\Delta\bar{i}_{\rm tcm}/\Delta t_{\rm dcm,on}$, and $\Delta\bar{i}_{\rm dcm}/\Delta t_{\rm tcm,on}$.

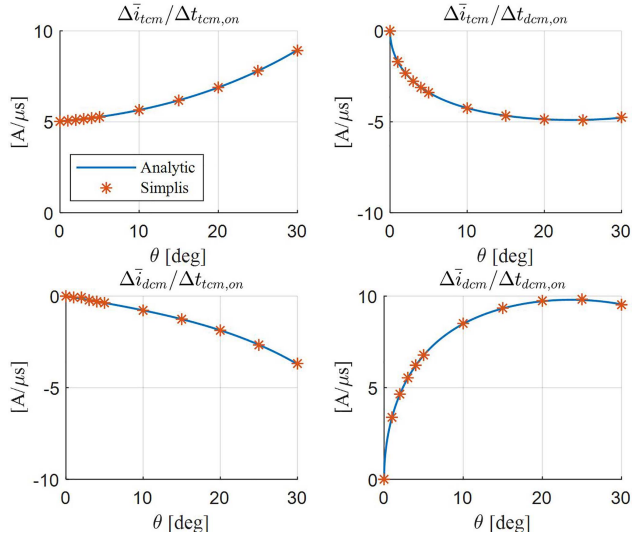

Fig. 8. Variance of low-frequency (<2 kHz) gain number according to θ.

the small signal dynamics under three-phase coupling for this modulation method.

VI. EXPERIMENTAL RESULT

A 30-kW three-phase NPC PV inverter has been built to verify the modeling approach and is shown in Fig. 9. The filter parameters are the same as Table VII, but the testing has been performed at 400 $V_{\rm dc}$ with 240 $V_{\rm ac}$. Due to delays in

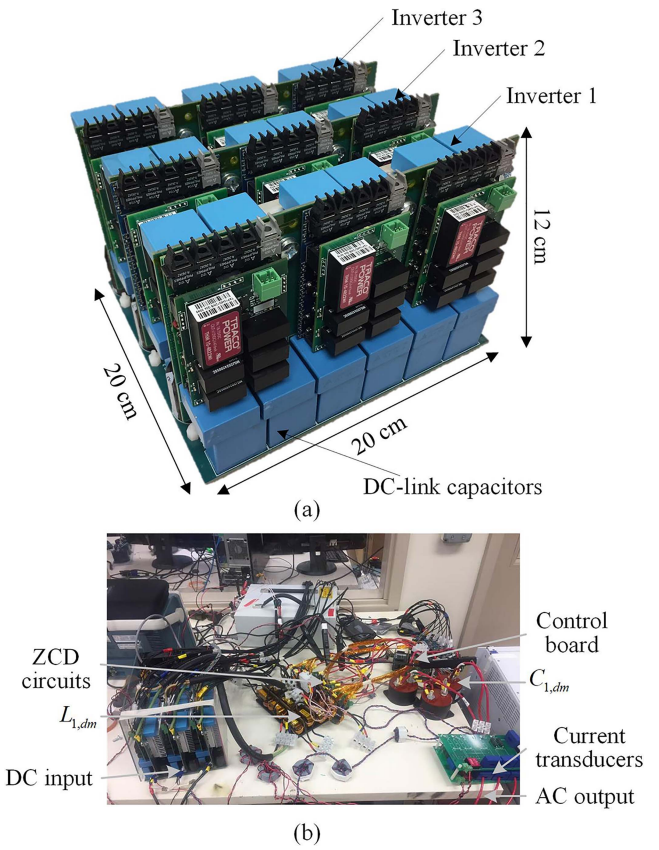

Fig. 9. (a) Prototype a 30-kW three-phase PV inverter operating in mixed conduction mode for ZVS operation. (b) Test setup.

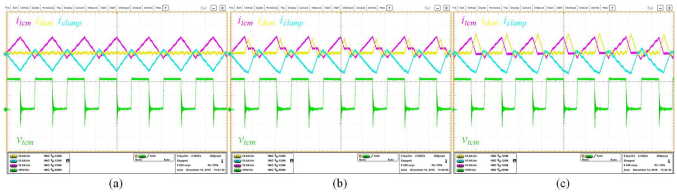

Fig. 10. Three-phase current waveform when grid angle is 15°: $t_{\mathrm{tcm,on}} = 4.0\ \mu$s, and $t_{\mathrm{dcm,on}}$ of (a) 0.0 μs, (b) 0.3 μs, and (c) 0.7 μs.

the zero-current detection circuit, fiber optics, and gate driver, t_R is 575 ns. When $t_{\mathrm{tcm,on}}$ is fixed to 4.0 μs, three different $t_{\mathrm{dcm,on}}$ are tested. As predicted by the model, t_{sw} remained as 7.2 μs irrespective of $t_{\mathrm{dcm,on}}$ as Fig. 10. Based on Table VI, the feedforward for $t_{\mathrm{tcm,on}}$ and $t_{\mathrm{dcm,on}}$ is used for CPLD in Fig. 1. The low-order harmonics meet IEEE 1547-2018 without any closed-loop compensator as shown in Fig. 11. At 60% load, total rated current distortion is 3.9%, and total harmonic distortion is 6.9%.

VII. Conclusion

This letter proposes single-phase equivalent circuits for the three-phase TCM inverter utilizing three different conduction modes for ZVS operation. Such an approach highly simplifies the modeling and analysis of the modulation. Also, given the current reference, analytic solutions can be derived without computational burden for small-signal gains or required ON-times

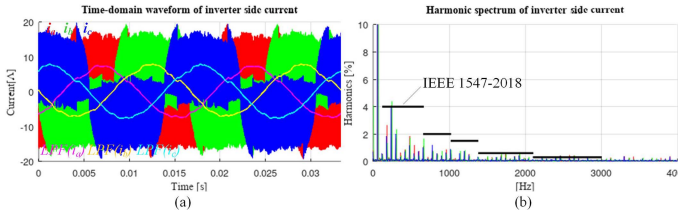

Fig. 11. (a) Inverter-side current with feed-forward terms on $t_{\mathrm{tcm,on}}$, and $t_{\mathrm{dcm,on}}$, which is calculated from the model. The operating point is at 400 V_{dc}, 8 A_{rms}. Low-pass filtered values are based on offline postprocess with 5 kHz cutoff frequency. (b) Harmonic spectrum of inverter current.

for the TCM and DCM phases. The validity of the proposed modeling approach has been verified with SIMPLIS simulation and experimental results. The presented modeling approach can be applied to the other switching sequences in [10], [11], and [12]. The proposed modeling can help engineers interpret the three-phase coupling and extend the control techniques for a single-phase TCM inverter toward WBG-based three-phase ZVS inverters.

References

[1] Z. Huang, Z. Liu, Q. Li, and F. C. Lee, "Microcontroller-based MHz totem-pole PFC with critical mode control," in *2016 IEEE Energy Convers. Congr. Expo.*, 2016, pp. 1–8.

[2] C. Marxgut, F. Krismer, D. Bortis, and J. W. Kolar, "Ultraflat interleaved triangular current mode (TCM) single-phase PFC rectifier," *IEEE Trans. Power Electron.*, vol. 29, no. 2, pp. 873–882, Feb. 2014.

[3] D. Rothmund, T. Guillod, D. Bortis, and J. W. Kolar, "99% efficient 10 kV SiC-Based 7 kV/400V DC-transformer for future data centers," *IEEE Trans. Emerg. Sel. Topics Power Electron.*, vol. 7, no. 2, pp. 753–767, Jun. 2019.

[4] J. Biela, D. Hassler, J. Miniböck, and J. W. Kolar, "Optimal design of a 5kW/dm3 / 98.3% efficient TCM resonant transition single-phase PFC rectifier," in *2010 Int. Power Electron. Conf. ECCE ASIA*, 2010, pp. 1709–1716.

[5] Z. Zhang, J. Zhang, S. Shao, and J. Zhang, "A high-efficiency single-phase T-type BCM microinverter," *IEEE Trans. Power Electron.*, vol. 34, no. 1, pp. 984–995, Jan. 2019.

[6] A. Amirahmadi et al., "Hybrid ZVS BCM current controlled three-phase microinverter," *IEEE Trans. Power Electron.*, vol. 29, no. 4, pp. 2124–2134, Apr. 2014.

[7] D. Leuenberger and J. Biela, "Comparison of a soft switched TCM T-type inverter to hard switched inverters for a 3 phase PV grid interface," in *2012 15th Int. Power Electron. Motion Control Conf.*, 2012, pp. LS1d.1-1–LS1d.1-8.

[8] A. Amirahmadi et al., "Hybrid ZVS BCM current controlled three-phase microinverter," *IEEE Trans. Power Electron.*, vol. 29, no. 4, pp. 2124–2134, Apr. 2014.

[9] Q. Zhang, H. Hu, D. Zhang, X. Fang, Z. J. Shen, and I. Bartarseh, "A controlled-type ZVS technique without auxiliary components for the low power DC/AC inverter," *IEEE Trans. Power Electron.*, vol. 28, no. 7, pp. 3287–3296, Jul. 2013.

[10] Z. Huang, Q. Li, and F. C. Lee, "Digital-based soft-switching modulation for high-frequency three-phase inverters with reactive power transfer capability," in *2018 IEEE Energy Convers. Congr. Expo.*, 2018, pp. 6751–6758.

[11] N. Haryani, S. J. Ohn, and R. Burgos, "ZVS turn-on triangular current mode (TCM) control for three-phase two-level converters with reactive power control," *IEEE Open J. Power Electron.*, vol. 4, pp. 923–933, 2023, doi: 10.1109/OJPEL.2023.3318997.

[12] Z. Huang, Q. Li, and F. C. Lee, "Critical-conduction-mode-based soft-switching modulation for three-phase PV inverters with reactive power transfer capability," *IEEE Trans. Power Electron.*, vol. 35, no. 6, pp. 5702–5713, Jun. 2020.

[13] S. Ohn, N. Haryani, R. Burgos, and D. Boroyevich, "A simplified digital closed-loop current control of three-phase PV inverter operating in triangular conduction mode," in *2019 10th Int. Conf. Power Electron. ECCE Asia*, 2019, pp. 2027–2033.